

## Morphology and tectonics of the Mid-Atlantic Ridge, 7°–12°S

N. J. Bruguier

Pembroke College, Cambridge, United Kingdom

T. A. Minshull

Southampton Oceanography Centre, Southampton, United Kingdom

J. M. Brozena

Marine Geosciences Division, Naval Research Laboratory, Washington, District of Columbia, USA

Received 7 September 2001; revised 10 July 2002; accepted 8 November 2002; published 13 February 2003.

[1] We present swath bathymetric, gravity, and magnetic data from the Mid-Atlantic Ridge between the Ascension and the Bode Verde fracture zones, where significant ridge-hot spot interaction has been inferred. The ridge axis in this region may be divided into four segments. The central two segments exhibit rifted axial highs, while the northernmost and southernmost segments have deep rift valleys typical of slow-spreading mid-ocean ridges. Bathymetric and magnetic data indicate that both central segments have experienced ridge jumps since  $\sim 1$  Ma. Mantle Bouguer anomalies (MBAs) derived from shipboard free air gravity and swath bathymetric data show deep subcircular lows centered on the new ridge axes, suggesting that mantle flow has been established beneath the new spreading centers for at least  $\sim 1$  Myr. Inversion of gravity data indicates that crustal thicknesses vary by  $\sim 4$  km along axis, with the thickest crust occurring beneath a large axial volcanic edifice. Once the effects of lithospheric aging have been removed, a model in which gravity variations are attributed entirely to crustal thickness variations is more consistent with data from an axis-parallel seismic line than a model that includes additional along-axis variations in mantle temperature. Both geophysical and geochemical data from the region may be explained by the melting of small ( $<200$  km) mantle chemical heterogeneities rather than elevated temperatures. Therefore, there may be no Ascension/Circe plume. *INDEX*

*TERMS:* 1517 Geomagnetism and Paleomagnetism: Magnetic anomaly modeling; 3010 Marine Geology and Geophysics: Gravity; 3040 Marine Geology and Geophysics: Plate tectonics (8150, 8155, 8157, 8158);

*KEYWORDS:* mid-ocean ridge, South Atlantic, crustal structure, gravity anomalies, swath bathymetry

**Citation:** Bruguier, N. J., T. A. Minshull, and J. M. Brozena, Morphology and tectonics of the Mid-Atlantic Ridge, 7°–12°S, *J. Geophys. Res.*, 108(B2), 2003, doi:10.1029/2001JB001172, 2003.

### 1. Introduction

[2] A variety of large-scale bathymetric anomalies occur along the global mid-ocean ridge system. Many of these are due to the interaction of ridges with nearby “hot spots.” The largest and most well-studied example of such interaction is Iceland, where the ridge axis rises above sea level and is underlain by a region of low mantle velocities interpreted as a hot plume [Wolfe *et al.*, 1997] which may extend throughout the mantle [Shen *et al.*, 1998; Bijwaard and Spakman, 1999]. Elsewhere, ridge-hot spot interactions are generally more subdued, and the smaller-scale interaction is commonly attributed to a larger distance between the ridge and the hot spot [Ito and Lin, 1995a; Kincaid *et al.* 1996]. However, even where bathymetric anomalies are relatively small, the presence of a near-ridge hot spot appears to give rise to significant changes in the morphology and tectonics of the ridge axis, with ridge

jumps and rift propagation more widespread [Brozena and White, 1990; Small, 1995]. While the evidence for a hot plume origin for the anomalies around Iceland appears strong, the origin of weaker long-wavelength axial depth anomalies remains controversial, with some authors favoring a chemical rather than thermal origin for these anomalies [e.g., Sleep, 1984; Shirey *et al.*, 1987; Michael *et al.*, 1994; Minshull *et al.*, 1998].

[3] In this paper we discuss the morphology and tectonics of the Mid-Atlantic Ridge between the Ascension and the Bode Verde fracture zones (Figure 1), where the spreading rate is 32–33 mm/yr [DeMets *et al.*, 1994], the axial depth anomaly reaches approximately +1 km, and significant residual depth anomalies extend several hundred kilometers to the east of the ridge axis [Minshull *et al.*, 1998]. These depth anomalies, and associated anomalies in the axial morphology [Brozena and White, 1990], geochemistry of axial basalts [Schilling *et al.*, 1985], and axial seismicity, are commonly attributed interaction between the mid-ocean ridge and the “Ascension” or “Circe” hot spot. Based on axial depth and geochemical anomalies and on off-axis

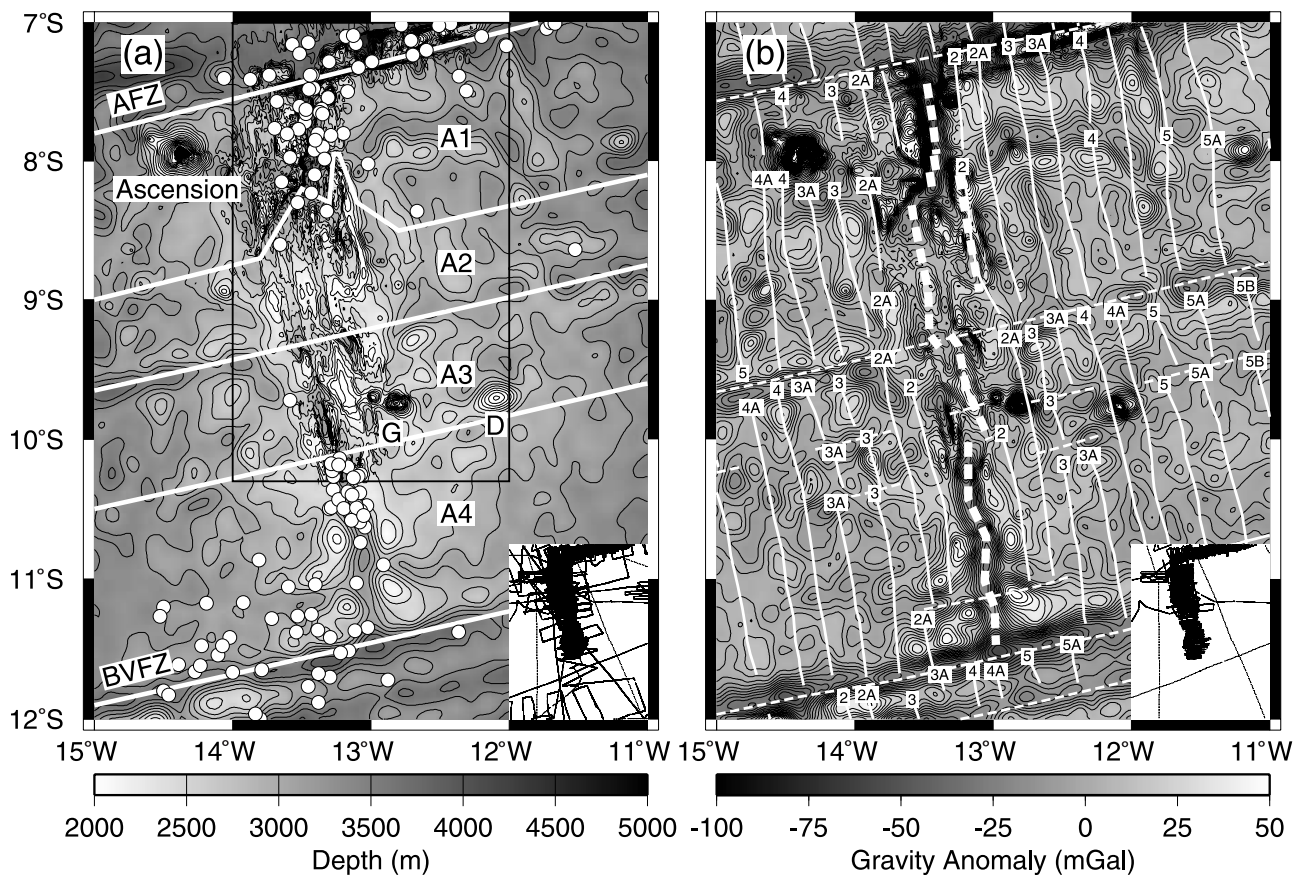


**Figure 1.** (a) Bathymetry of the Mid-Atlantic Ridge between the Ascension and the Bode Verde fracture zones. Swath data at the ridge axis were combined with archived single beam echosounder profiles and satellite gravity-derived bathymetry, following the procedure outlined by *Minshull et al.* [1998]. Grid interval is 0.01 and contour interval is 200 m. The apparently rougher area around the ridge axis in segments A1–A3 is the area covered by swath bathymetry. White circles mark earthquakes of body wave magnitude 4.1 or greater, during 1964–1999, with a typical uncertainty of 5–10 km [International Seismological Centre, 2001]. Thick white lines mark boundaries of segments described in the text. AFZ is the Ascension Fracture Zone, BVFZ is the Bode Verde Fracture Zone, G marks Grattan seamount, and D marks Seamount D of *Brozena* [1986]. Circe seamount lies within segment A2 at  $\sim 9^{\circ}20'W$ . Box marks area of gravity analysis (Figures 11 and 12). Inset shows ship tracks used in the calculation of the long-wavelength component of the bathymetry. (b) Combined shipboard and satellite free air gravity for the same region. Contour interval is 5 mGal. Thick dashed white lines mark inferred ridge axis location (this paper), thin solid white lines mark magnetic anomaly picks of *Brozena* [1986], and thin dashed white lines mark fracture zone picks of *Brozena* [1986]. Inset shows shipboard gravity data used in the compilation.

residual depth anomalies, the hot spot has been identified with a significant off-axis plume with a volumetric flux and buoyancy flux about half that of Iceland [Davies, 1988; Schilling, 1991; Malamud and Turcotte, 1999]. However, these flux estimates either ignore the contribution of crustal thickening to the depth anomalies, or assume that the contribution is negligible. If instead the anomalies are attributed entirely to Airy compensation of igneous addition to the crust between the Ascension and the Bode Verde fracture zones in the last 25 Myr, the long-term average melt production required is only  $0.017 \text{ km}^3/\text{yr}$  [Minshull et al., 1998], which is much smaller than estimates for robust on-axis plumes such as Iceland.

[4] An additional point of controversy has been the location of the hot spot in this region. Several large seamounts are present on both the western and eastern flanks of

the ridge axis [Brozena, 1986]. Schilling et al. [1985] speculated that the hot spot was located 450 km east of the ridge axis at a truncated topographic bulge around Circe seamount. However, recent  $^{40}\text{Ar}/^{39}\text{Ar}$  dating of rocks from Circe seamount suggest an age of  $6.6 \pm 0.1 \text{ Ma}$  [O'Connor et al., 1999], indicating that the seamount is not the site of recent volcanism. Basalts from the ridge axis have Pb isotopic anomalies which do not fall on a mixing trend between mid-ocean ridge basalt (MORB) and Ascension Island compositions [Hanan et al., 1986], indicating that the geochemical anomaly at the ridge axis is unrelated to Ascension Island, and that the mantle source of the geochemical anomalies is more likely located east of the ridge axis. Brozena [1986] suggested a hot spot location close to the ridge in the region of Grattan seamount and seamount D (Figure 1). This suggestion has received recent support from

Pb isotopic measurements on basalts dredged from Grattan [Bourdon and Hémond, 2001], which indicate that they may form the “missing end-member” of the mixing trend identified by Hanan *et al.* [1986]. Finally, using a local velocity for the African plate relative to a “fixed” hot spot frame that is based on the St Helena seamount chain, O'Connor *et al.* [1999] suggest a present-day hot spot location 130 km southwest of Circe seamount, where there is also a significant residual depth anomaly [Minshull *et al.*, 1998].

## 2. Regional Tectonic Setting

[5] Based on aeromagnetic data, Brozena [1986] identified three ridge offsets between the Ascension and the Bode Verde fracture zones (Figure 1). As observed at several other locations [e.g., Tucholke *et al.*, 1997], the pattern of ridge axis segmentation has remained stable over time despite variations in the magnitude of the offsets, at least since magnetic anomaly 5C (16 Ma, according to the timescale of Cande and Kent [1995], which is used throughout this study). These three second-order offsets divide the ridge into four spreading segments, labeled A1–A4 in this study. The most northerly offset cuts the ridge axis near 8°20'S, and displaces left-laterally all anomalies out to anomaly 2A (3 Ma). Between anomaly 2A and anomaly 4A, the offset disappears. Before anomaly 4A (9 Ma), there is a right-lateral offset in the anomalies which coincides with weak gravity lows on both flanks of the ridge axis (Figure 1) [Mello, 1993]. The second long-lived offset is a right-lateral offset at 9°20'S (fracture zone A of Brozena [1986]). This offset also coincides with a linear gravity low on both flanks of the ridge. The third offset at 10°S is also right lateral at present, but the sense of offset appears to have changed over time and there is no corresponding gravity lineation. Two smaller offsets of the central anomaly near 8°S and 11°S appear to be more short-lived features.

[6] Using the timescale of LaBrecque *et al.* [1977], Brozena [1986] inferred large variations in spreading rate over the past 16 Ma, including a dramatic increase between 10 and 7 Ma and a decrease from 6 to 2 Ma. Much of this variation can be attributed to inaccuracies in the magnetic anomaly timescale: Cande and Kent [1992] demonstrated that errors existed in all previous timescales which are inherited from the original work of Heirzler *et al.* [1968], and that anomaly 5 was approximately 1.0 Ma too young in the timescale of LaBrecque *et al.* [1977]. Using the revised timescale of Cande and Kent [1995], we infer that the spreading rate varies much more smoothly, with a gradual decrease in spreading rate from 48 to 32 mm/yr between 11 and 4 Ma and a roughly constant rate of 32–33 mm/yr since 4 Ma (Figure 2), in agreement with the NUVEL-1A model [DeMets *et al.*, 1994]. Before 10 Ma, there was significant (~20%) asymmetry in the spreading rates, with the east flank spreading at ~21 mm/yr and the west flank at ~26 mm/yr, but since 10 Ma spreading has been symmetric. The present apparent asymmetry of ~12% is due primarily to an eastward ridge jump that has occurred since anomaly 2 time [Brozena and White, 1990].

## 3. Ridge Axis Morphology

[7] Here we interpret in detail a bathymetric grid constructed from the swath data set of Brozena and White

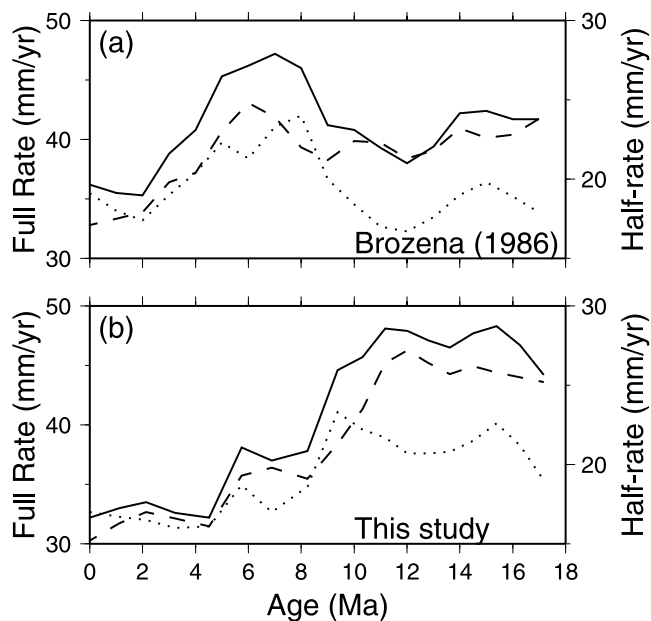


**Figure 2.** Spreading rate versus time for the east flank (dotted line), west flank (dashed line), and total rate (solid line): (a) values obtained by Brozena [1986] using the magnetic anomaly timescale of LaBrecque *et al.* [1977] and (b) recalculated values using the timescale of Cande and Kent [1995]. Values are 2 Ma running averages, with the exception of the value from 0 to 1 Ma, which is plotted at zero age.

[1990], and use these data with the magnetic data analysis in the following section to locate the present-day spreading center. Swath survey lines ran predominantly E-W across the ridge axis at ~3 km spacing, to give ~80% bathymetric coverage.

### 3.1. Segment A1

[8] Ridge segment A1 is ~90 km long and is characterized by a well-defined, continuous rift valley with over 1000 m of relief, and significant seismicity (Figures 1 and 3). The ridge–transform intersection is marked by a deep, triangular nodal basin with a maximum depth of 5100 m and a width of ~25 km. The basin is truncated abruptly to the north by a steep, linear scarp over 1000 m high, interpreted to mark the trace of the active transform fault. To the east of this basin is a shallow inside corner high, rising to a depth of 1100 m. The rift valley shallows and narrows southward toward the segment center, reaching a minimum depth of 3400 m and a width of ~5 km at 7°53'S. Further south, the valley deepens and widens again, reaching depths of 3700–4000 m. The center of the rift valley floor at 8°S is marked by a linear ridge, several hundred meters high and ~10 km long. Another similar ridge appears further south at 8°10'S, offset 5 km to the west. We interpret these ridges as sites of recent constructional volcanic activity at the plate boundary.

[9] Flanking the axial valley, the rift valley walls rise in a series of terraces bounded by steep fault scarps. The rift mountains show considerable asymmetry: away from the inside corner high, the east flank rises to a minimum depth of 2100 m, whereas the west flank is shallower, rising to

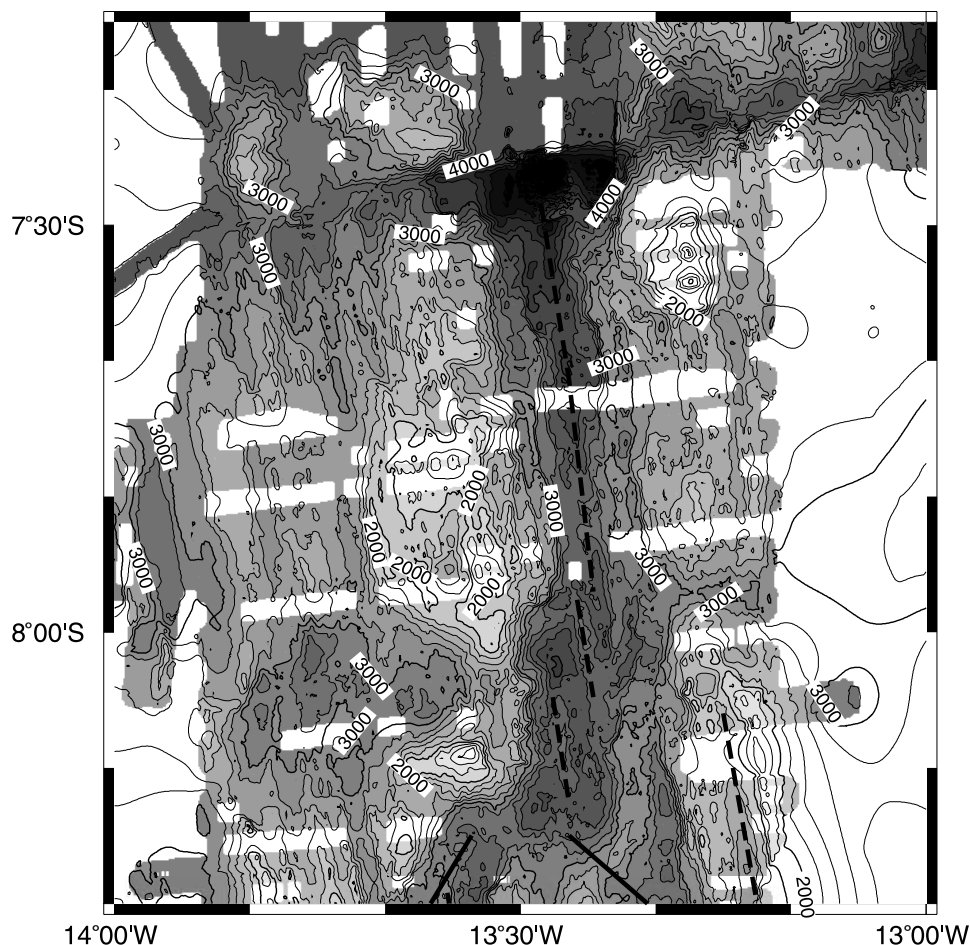


**Figure 3.** Gridded SeaBeam bathymetry of segment A1. Contour interval is 200 m. Outside the region of SeaBeam coverage, data from Figure 1 are contoured. Dashed lines show interpreted location of present-day plate boundary. Solid lines mark pseudofault traces formed by northward propagation of segment 2.

1600 m. A circular, closed-contour depression at 7°55'S, 13°35'W was interpreted by *Brozena and White* [1990] as a large caldera 300–400 m deep topping a circular volcanic platform; this feature suggests the presence of ongoing off-axis volcanism [*Klingelhofer et al.*, 2001].

### 3.1.1. 8°15'S Discontinuity

[10] The 8°15'S discontinuity represents a right-lateral offset in the ridge axis of ~20 km (Figures 3 and 4). At the southern end of segment A1, where it intersects the discontinuity, the axial valley deepens to form a 3800 m basin trending obliquely to the ridge axis. The intersection of the western spreading axis in segment A2 (see below) with the discontinuity is marked by a similar basin reaching 3600 m depth. The off-axis trace of the discontinuity forms a discordant zone, which disrupts the ridge-parallel seafloor fabric. On the western flank of the ridge, this zone consists of a series of deep basins trending NE-SW, at ~45° to the spreading direction, suggesting that the offset has been migrating northward at a rate approximately equal to the half-spreading rate of the ridge [*Brozena and White*, 1990], since at least 4 Ma.

[11] The discordant zone is bounded to the north by a steep scarp with ~1800 m of relief. A shallow inside corner high rising to a minimum depth of 1400 m can be seen to

the north of the discontinuity at 8°10'S, and the summit of the scarp is the off-axis expression of the inside corner highs formed at the southern tip of segment A1. A conjugate series of basins can be seen on the east flank of the ridge, trending NW-SE, with a similar region of shallow bathymetry to the south of these basins which represents the relict inside corner highs formed at the northern tip of segment A2. This ridge is less distinct, probably because of the deformation that must have occurred in the zone of transferred lithosphere formed as the discontinuity migrated northward [*Hey et al.*, 1980]. Magnetic anomaly data suggest that a recent eastward ridge jump of segment A2 has reversed the sense of ridge offset, and the discontinuity is now a left-lateral offset of 20–25 km [*Brozena and White*, 1990].

### 3.2. Segment A2

[12] Two ridge axes may be defined in segment A2 (Figure 4); on the basis of magnetic modeling (see below), the eastern axis is interpreted as the current spreading center in the north of the segment, whereas the western axis may still be active in the south. The segment appears to be magmatically inflated, and exhibits very little seismicity (Figure 1). The eastern axis has a shallow rift valley, while

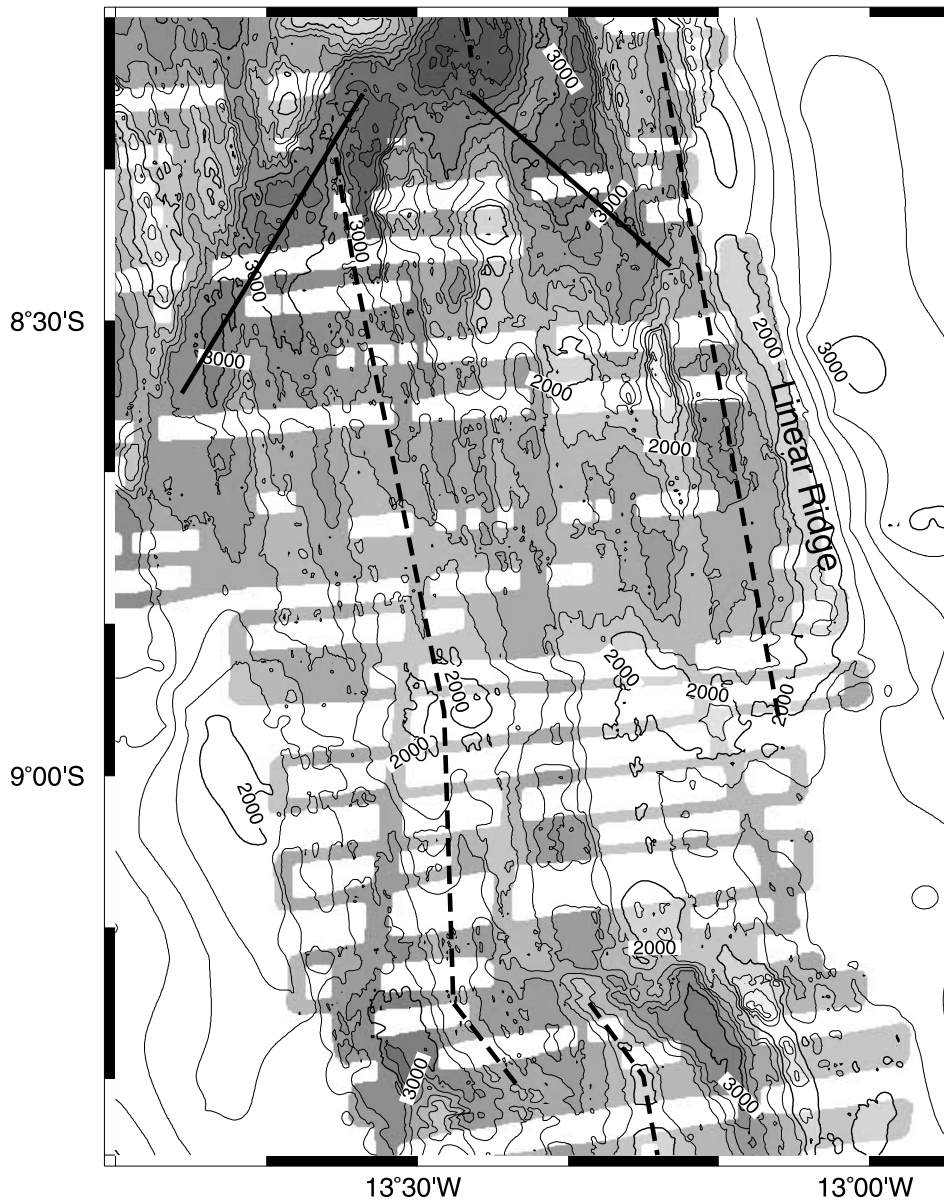


**Figure 4.** Gridded SeaBeam bathymetry of segment A2, plotted as in Figure 3. The “linear ridge” of *van Andel and Heath* [1970] is marked.

the western axis has a rifted axial high reaching a minimum depth of 2000 m. Conjugate highs are located  $\sim 25$  km either side of the western axis, perhaps representing a previous phase of magmatic inflation. The most striking feature of the eastern axis is a large, linear ridge running parallel to the axis between  $8^{\circ}5'S$  and  $9^{\circ}S$ , which rises to a depth of less than 2000 m. This ridge is continuous across the pseudofault trace, suggesting that it is a relatively recent feature that has overprinted the preexisting terrain. The ridge is interpreted as the eastern wall of the rift valley, bounded by steep fault scarps. The western wall is generally less well developed, except at  $8^{\circ}35'S$  where it rises to a minimum depth of 1400 m.

### 3.2.1. $9^{\circ}20'$ Discontinuity

[13] The boundary between segments A2 and A3 is marked by a 15 km left-lateral offset (Figures 4 and 5). Here, the rifted high forming the southern end of segment

A2 and the axial ridge which forms the spreading center of segment A3 curve toward each other and overlap by  $\sim 10$  km. The morphology is similar to that exhibited by overlapping spreading centers (OSCs) on the East Pacific Rise [MacDonald *et al.*, 1988] and elsewhere in the Atlantic [Grindlay *et al.*, 1991]. Two overlap basins formed at the OSC and rafted away are visible either side of the ridge axis, with depths in excess of 3000 m.

### 3.3. Segment A3

[14] Segment A3 is the shallowest segment (Figure 5), and here the spreading center is marked by an axial high  $\sim 70$  km in length. The ridge axis in this segment is devoid of teleseismically detectable earthquakes (Figure 1). South of the OSC, the axial high widens and shallows to reach a minimum depth of 1460 m and a width of  $\sim 20$  km at  $9^{\circ}36'S$ . Two large off-axis seamounts appear to the east of

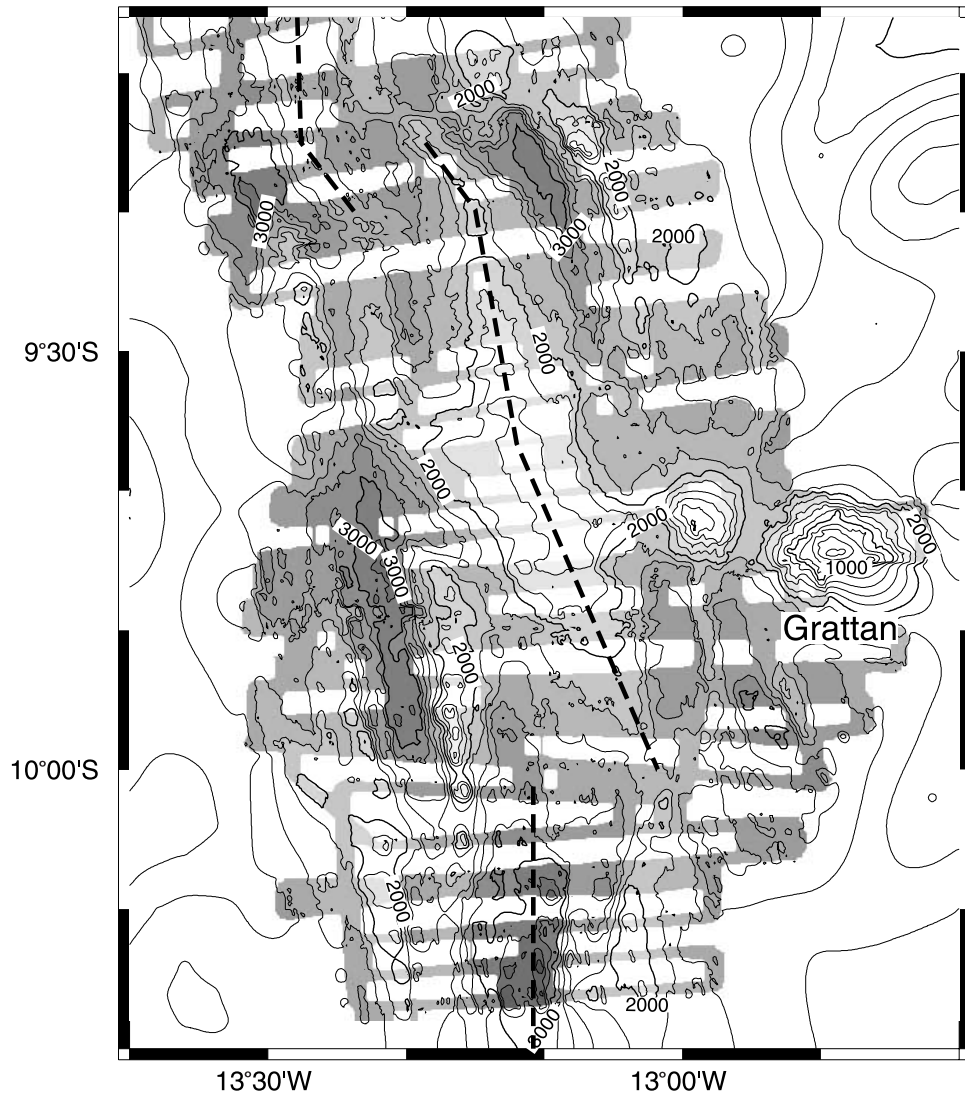


**Figure 5.** Gridded SeaBeam bathymetry of segment A3, plotted as in Figure 3. No swath data were acquired to the south of the area shown.

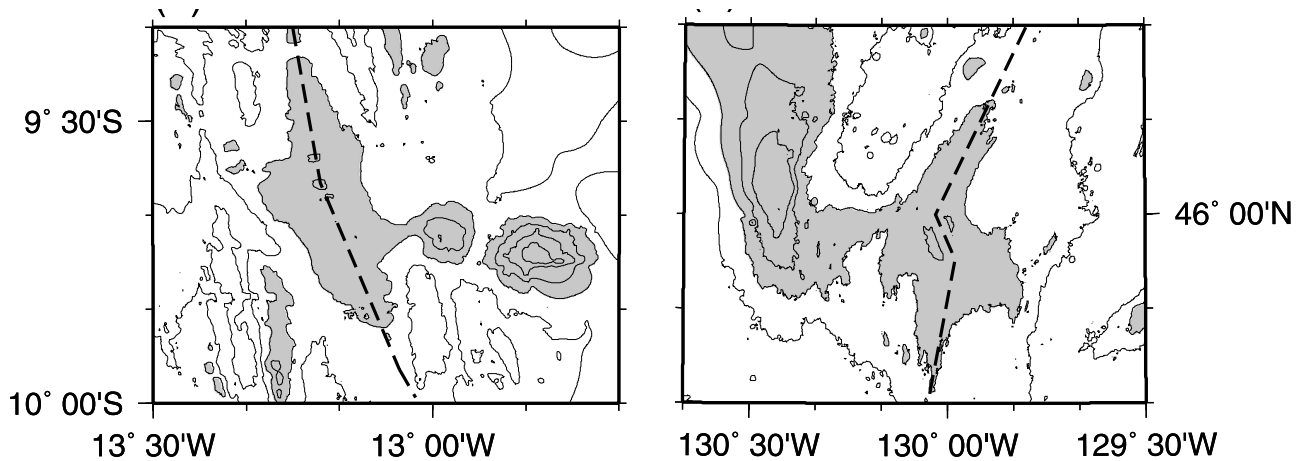


**Figure 6.** Comparison between (a) ridge segment A3 and (b) Axial Seamount on the Juan de Fuca Ridge at the same scale. Contour interval is 500 m. Bathymetric features shallower than 2000 m are shaded. Dashed line marks the spreading axis.

the ridge axis. The seamount at 9°42'S, 12°59'W is 19 km from the axis and rises to a minimum depth of 1100 m. Grattan Seamount is 35 km east of the axis at 9°44'S, 12°49'W and rises to a depth of just 72 m. On the west flank of the ridge axis between 9°40' and 10°5'S there is a ~9 km wide valley reaching a depth of 3100 m and flanked by linear ridges rising to ~1500 m; we interpret this feature as a rift valley abandoned by a recent eastward ridge jump. A similar deep valley flanked by a shallow linear ridge is visible on the east flank between 9°10' and 9°30'S. The two valleys may once have been continuous and have been subsequently dissected by the new spreading center. The offset between them is now ~35 km, suggesting that the excess volcanism forming the present axial high has occurred since ~1 Ma. Segment A3 is similar in both size and shape to Axial Seamount on the Juan de Fuca Ridge (Figure 6), which is both volcanically and hydrothermally active, is topped by a large, elongated caldera, and has several large off-axis seamounts nearby [Johnson and Embley, 1990]. Magnetic anomaly data suggest that there has also been a recent ridge jump at Axial Seamount [Delaney et al., 1981].

### 3.3.1. 10°S Discontinuity

[15] The 10°S discontinuity is a ~15 km right-lateral offset (Figure 5) formed by the recent ridge jump of segment A3. There was probably no offset immediately prior to this ridge jump, though a discontinuity at this latitude has been present since ~14 Ma (Figure 1) [Brozena, 1986].

### 3.4. Segment A4

[16] Segment A4 (Figure 1) is the longest of the four segments, but Seabeam data are only available from its northernmost part. This segment has a well-defined rift valley with a depth of ~3400 m and a width of ~10 km, and significant seismicity. The flanking rift mountains rise to depths of less than 2000 m. The sinuous appearance of the rift valley may indicate the presence of several unresolved small offsets.

## 4. Magnetic Data

[17] The most pronounced feature of magnetic data from the area (Figure 7) is a broad linear positive anomaly in segment A2, interpreted as the Bruhnes anomaly associated with the western spreading axis. The highest-amplitude anomalies coincide with the ridge axis discontinuities at 8°15'S and 9°20'S, a phenomenon which has been attributed elsewhere to Fe-Ti enrichment of the erupted basalts by extensive shallow-level fractionation [Vogt, 1979]. The offset of the Bruhnes anomaly to the east of the axial high in the northern part of segment A3 and to the west of the axial high in the southern part of this segment provides further evidence for a recent ridge jump in this segment.

[18] Based on magnetic profiles across the northern half of segment A2, van Andel and Heath [1970] picked the ridge axis at 13°15'W from the combination of a high-amplitude magnetic anomaly and bathymetric evidence for a linear ridge (marked in Figure 4). An independent constraint comes from a dredge sample described by the same authors. They report that late Pliocene (3.5–2.0 Ma) baked foraminiferal ooze was discovered on a basalt boulder dredged from the west flank of the linear ridge, in conflict

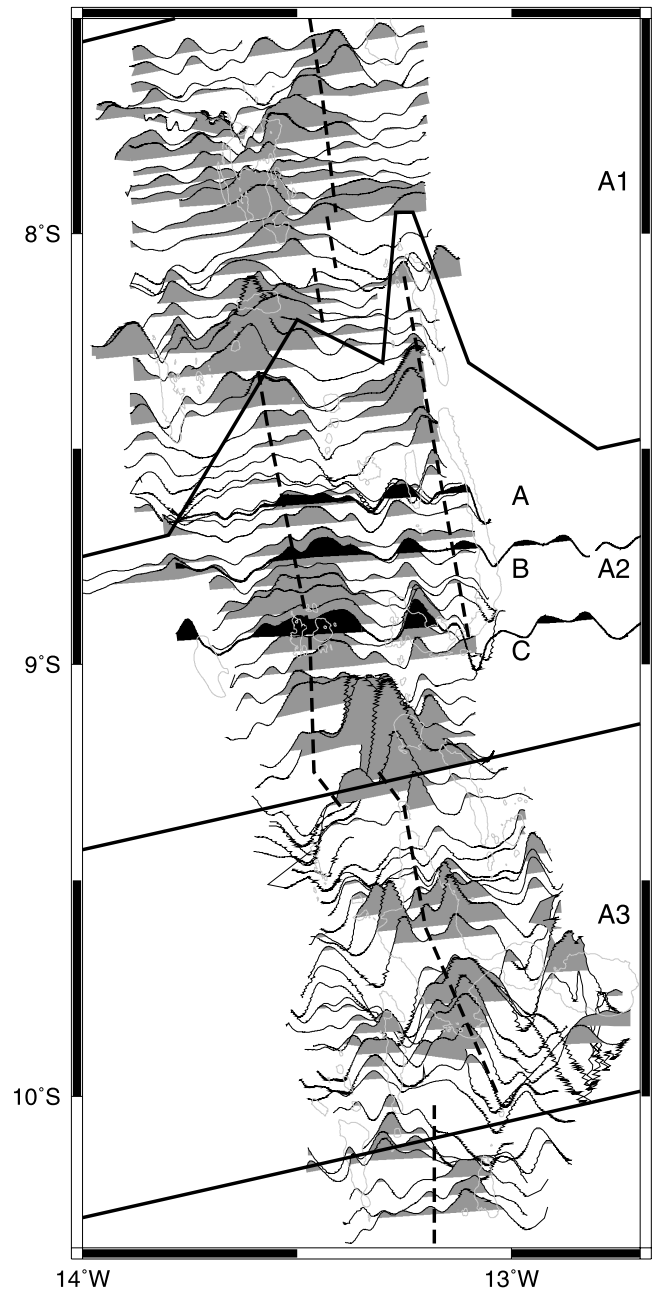


**Figure 7.** Magnetic anomaly data plotted along ship tracks. Black shaded profiles labeled A–C are modeled in this paper. Data are reduced to the appropriate IGRF and plotted with a bias, which reduces profile averages to zero. Pale gray lines mark the 2000 m bathymetric contour, thick dashed line marks spreading axis, and thick solid lines mark segment boundaries.

with their magnetic anomaly interpretation, which predicts an age of 0.7 Ma for this ridge. They also observed up to 200 m of sediment in the valley immediately east of the linear ridge. Generally, however, they observed very little sediment cover, suggesting that magnetic anomalies could be adequately modeled using the seabed as the top of the magnetized layer.

[19] Based on an inversion for magnetization [Parker and Huestis, 1974] of the data shown in Figure 7 and an

association of high magnetization with recent volcanism, *Brozna and White* [1990] identified three neovolcanic segments within segment A2, which overlap by  $\sim 10$  km and are each associated with topographic ridges interpreted as constructional volcanic features. However, the inversion for magnetization can become unstable close to the magnetic equator because any small N-S lineated features in the observed field will result in large-amplitude N-S features in the magnetization solution [Miller and Hey, 1986]. Here, we investigate the recent spreading history of segment A2 by forward modeling of three long E-W magnetic profiles acquired in 1993 (Figure 7); elsewhere, magnetic profiles are generally too short for forward modeling to be useful.

[20] Synthetic magnetic anomaly data were generated using a two-dimensional approach which incorporates the observed bathymetry, the azimuth of the spreading center and a magnetic reversal timescale [Naar and Hey, 1986]. The spreading rate and times and distances of discrete ridge jumps were considered as free parameters. Results from three different models were compared. The first attempts to fit the data with a constant spreading rate and no ridge jumps (Figure 8). This results in a good fit to the central anomaly and to anomaly 2, particularly for profile C, but prior to anomaly 2, the fit is poor. Matching the earlier anomalies by changes in spreading rate alone requires unrealistically large variations over short time intervals; we conclude that one or more ridge jumps are required to fit the data.

[21] Our second model was that of *Brozna and White* [1990], who identified the high-amplitude, narrow anomaly near the center of the profiles as the current spreading axis and two weak anomalies to the west as anomaly 2 either side of an extinct spreading center. An initial model was constructed using the times and distances of ridge jumps inferred by *Brozna and White*, and these parameters were then adjusted to optimize the fit (Figure 9). The optimized model includes a ridge jump at 1.3 Ma, which affected profiles A and B only, and a further jump at 0.3 Ma, which affects all three profiles. The model matches well the eastern half of profile B, suggesting that anomalies 2A and 3 have been correctly identified, but the match to the western half of the profiles is generally worse than for the model without ridge jumps. Although variations in magnetization, which are not accounted for in the model, may explain some of the discrepancy, the overall shape of the anomalies will not be affected by smooth lateral changes in magnetization. A further problem with this model is that the magnetization high coincides with the location of *van Andel and Heath's* [1970] Pliocene dredge sample.

[22] A simpler model that provides a better overall fit to the data has a single ridge jump by 35 km to the east at 0.3 Ma and a constant half-spreading rate of 18 mm/yr (Figure 10). Anomalies 2 and 2A are then well matched on all three profiles. The positive anomaly between anomalies 2 and 2A is interpreted as the location of the current spreading center, and is well matched on profiles A and B. A negative anomaly appears at this location in profile C, where the southern end of the linear ridge curves to the west; it is possible that the most recent spreading has been accommodated tectonically in this region, with insufficient volcanism to produce a positive anomaly. This new model has the  $9^{\circ}15'$  discontinuity as a right-lateral offset prior to the ridge jump, as suggested by the bathymetry.

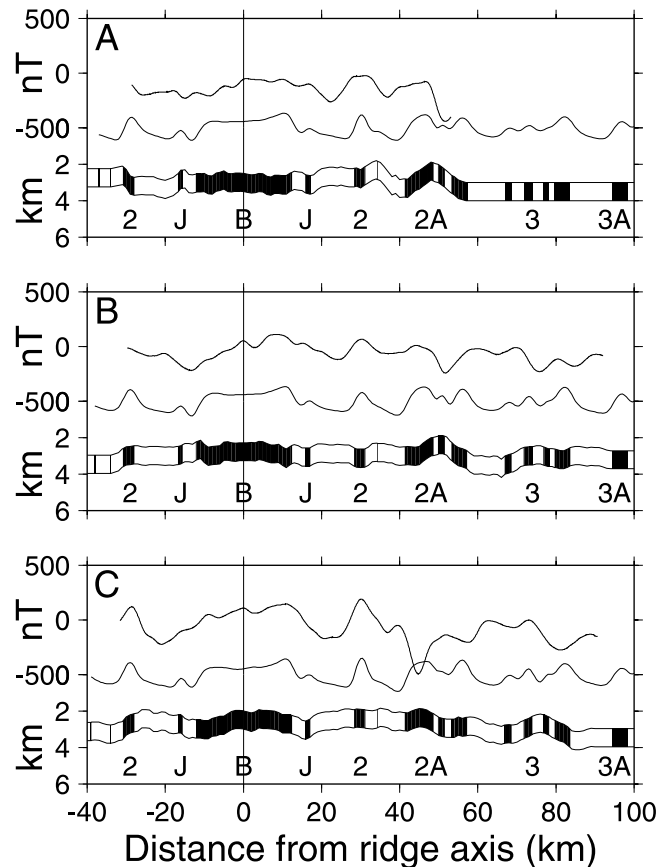


**Figure 8.** Magnetic anomaly profiles and models for segment A2 with a constant half-spreading rate of 16 mm/yr. For each of the three profiles marked in Figure 7, the observed data (top) and synthetic data (middle) are shown with the magnetization model, which consists of a 1 km magnetic source layer with an effective susceptibility of 0.02, bounded at its top by the seabed. Dark blocks are normally magnetized. Labels below the models mark the Bruhnes (B), Jaramillo (J), and other numbered magnetic anomalies. The reversal pattern is based on the magnetic reversal timescale of *Cande and Kent* [1995].

[23] The linear ridge at  $13^{\circ}15'W$  forms the eastern wall of the new rift valley and has a modeled age of  $\sim 2.5$  Ma, in good agreement with the age of the dredge sample. The  $\sim 10$  km width of the rift valley corresponds to  $\sim 0.3$  Myr of spreading. The western wall is less well developed (Figure 4), perhaps because the lithosphere there is younger and thinner than to the east [Chen and Morgan, 1990], or because the topography is generated by reactivation of normal faults generated at the western spreading center. Such faults would dip predominantly to the west, which is the right direction for reactivation on the eastern flank of the new spreading center, but in the wrong direction for reactivation on the western flank.

## 5. Gravity Data

[24] An extensive gravity data set was acquired for segments A1–A3. An initial interpretation of these data, focused on segment A2, was given by *Minshull et al.*

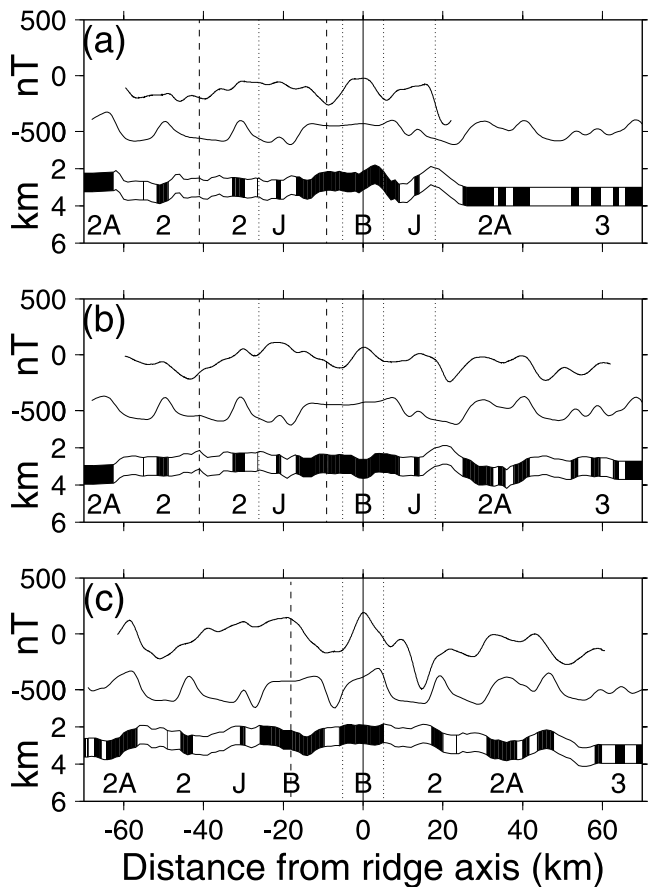


**Figure 9.** Magnetic anomaly profiles and models for segment A2 for the spreading history proposed by *Brozena and White* [1990] and a half-spreading rate of 17 mm/yr. Model parameters are as for Figure 8. Vertical solid lines indicate the current spreading center, dotted lines indicate age discontinuities (pseudofaults) resulting from ridge jumps, and dashed lines indicate failed rifts.

[1998]. Following a crossover error analysis, which gave a final root-mean-square crossover error of 2.9 mGal [*Minshull et al.*, 1998], shipboard data were combined with satellite data [*Sandwell and Smith*, 1997] for points more than 0.1' from the nearest shipboard measurement, and the combined data set was interpolated onto a 0.01° grid interval (Figure 1b). Prior to combining the data, the mean difference between satellite and shipboard values was computed along ship tracks, and the shipboard data were adjusted to set this difference to zero.

[25] A mantle Bouguer anomaly (MBA) (Figure 11) was then computed using water, crust and mantle densities of 1.03, 2.86, and 3.33 mg/m<sup>3</sup>, respectively, and a reference crustal thickness of 7 km. Gravity calculations used the Fourier-based approach of *Parker* [1973], and covered an area of 5.12° × 5.12°, much larger than the region shown in Figure 11, to eliminate edge effects. Our analysis is focused on the region of good bathymetric coverage, since outside this region the bathymetry used from gravity corrections is itself derived from satellite gravity data [*Minshull et al.*, 1998]. The crustal density used is the estimated mean value for oceanic crust of *Carlson and Herrick* [1990]. The MBA is relatively insensitive to variations in this value, with a

difference of less than 2 mGal resulting everywhere except at the largest seamounts (e.g., Grattan) if the more common value of 2.80 mg/m<sup>3</sup> is used instead.

[26] The strongly negative free air anomaly along the median valley of segment A1 is almost completely removed by the mantle Bouguer correction, indicating that the rift valley is not isostatically compensated across-axis and that the assumption of constant crustal thickness is probably a fair approximation within the segment. Two distinct sub-circular gravity lows appear in segments A2 and A3, similar to the “bull’s-eye” anomalies observed elsewhere on the Mid-Atlantic Ridge [e.g., *Kuo and Forsyth*, 1988]. In segment A2, the negative anomaly is centered on the eastern ridge axis. If the magnetic anomaly model of Figure 10 is correct, the ridge jump occurred into ~2 Ma lithosphere, which would have a thickness of ~20 km [e.g., *Parsons and Sclater*, 1977]. The thermal time constant of a 20 km lithosphere is ~1.3 Ma, so the location of MBA minimum would then suggest that lithospheric thinning and associated mantle upwelling occurred beneath the eastern ridge axis long before the surface expression of the ridge jump at 0.3 Ma. If the surface expression of the ridge jump occurred much earlier, as in the model of *Brozena and White* [1990], such a time difference is not required. In segment A3, the negative anomaly is also centered on the present ridge axis, though small residual lows are present to the west of the southern part of the axis and to the east of the northern part.

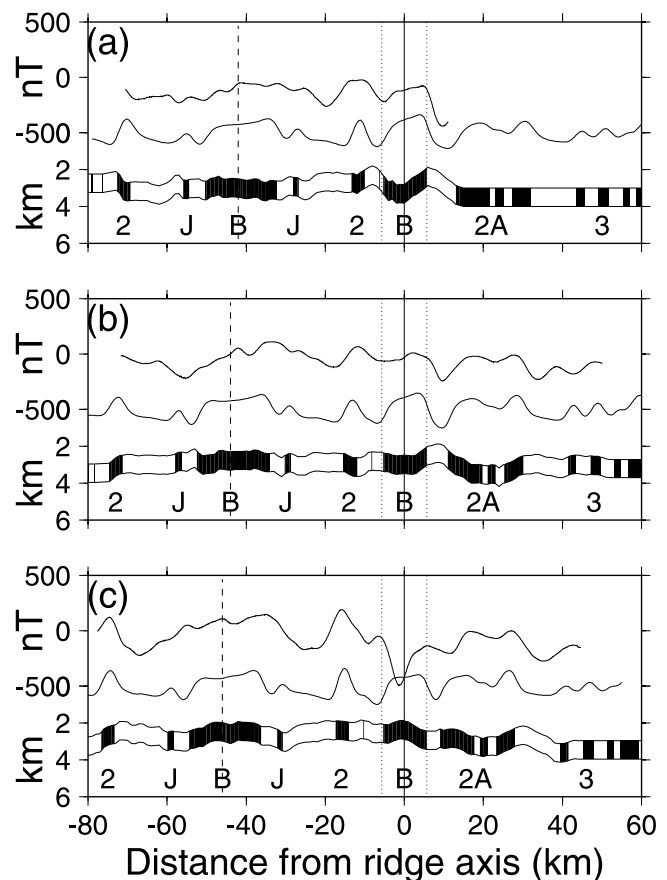


**Figure 10.** Magnetic anomaly profiles and best fitting forward models for segment A2. Model parameters are as for Figure 8 and vertical lines as for Figure 9.

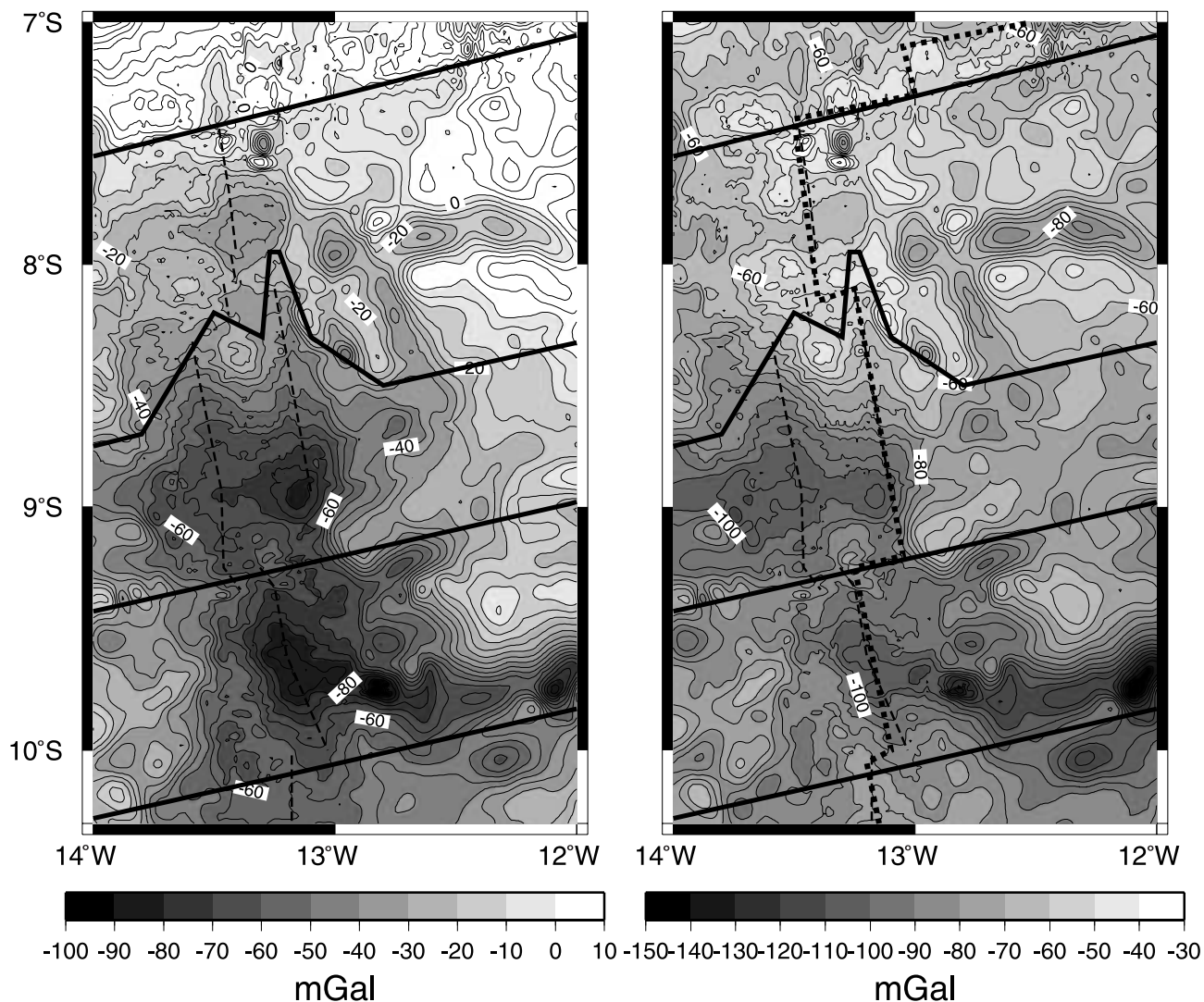


**Figure 11.** (a) MBA calculated by removing from the free air gravity anomaly of Figure 1b the predicted gravitational attraction of the seabed and a constant density, 7 km thick crust. Contour interval is 5 mGal. Thick solid lines mark segment boundaries and dashed line marks current spreading center. (b) Residual MBA after subtracting predicted gravitational attraction of the thermal model described in the text. Contour interval is 5 mGal. Solid and dashed lines are as in (a) and thick dotted line marks the simplified plate boundary used in the thermal calculation.

[27] The MBA is dominated by a general increase in gravity away from the ridge axis due to lithospheric cooling. To emphasize deviations from this pattern, we removed the predicted gravity effects of a simple thermal model based on the three-dimensional passive flow model of *Phipps Morgan and Forsyth* [1988]. In the model, the spreading system is described by a series of straight, orthogonal ridges and transforms, so ridge jumps and rift propagation cannot be accounted for explicitly. The spreading center was approximated by the boundary shown in Figure 11b. The temperature field was computed on a  $512 \times 512$  grid with a grid spacing of 2 km, using reference temperatures of  $0^\circ\text{C}$  at the seabed and  $1300^\circ\text{C}$  at 100 km depth. The edges of the grid are at least 450 km from ridges and 250 km from transforms, so that edge effects in the region of interest are negligible. The model used a half-spreading rate of 18 mm/yr. The density distribution in the mantle was determined

from the temperature field using a thermal expansion coefficient of  $3.2 \times 10^{-5}/^\circ\text{C}$ .

[28] The residual anomaly (RMBA) (Figure 11b) reflects deviations in crustal thickness and crust and mantle density from those assumed in the model. The main features are broad lows centered on the west flank of the ridge axis at the center of segment A2, and on the east flank at the center of segment A3, with other lows around off-axis seamounts. The low west of segment A2 could be due to the residual thermal effect of the abandoned spreading center, which is not accounted for in the thermal model. An end-member model is to assume that the RMBA results entirely from variations in crustal thickness. The thickness variations required were computed by downward continuation of the RMBA to a depth of 10 km, corresponding to a typical water depth of 3 km and a crustal thickness of 7 km, and scaling by the density contrast of  $0.47 \text{ mg/m}^3$  at the base of

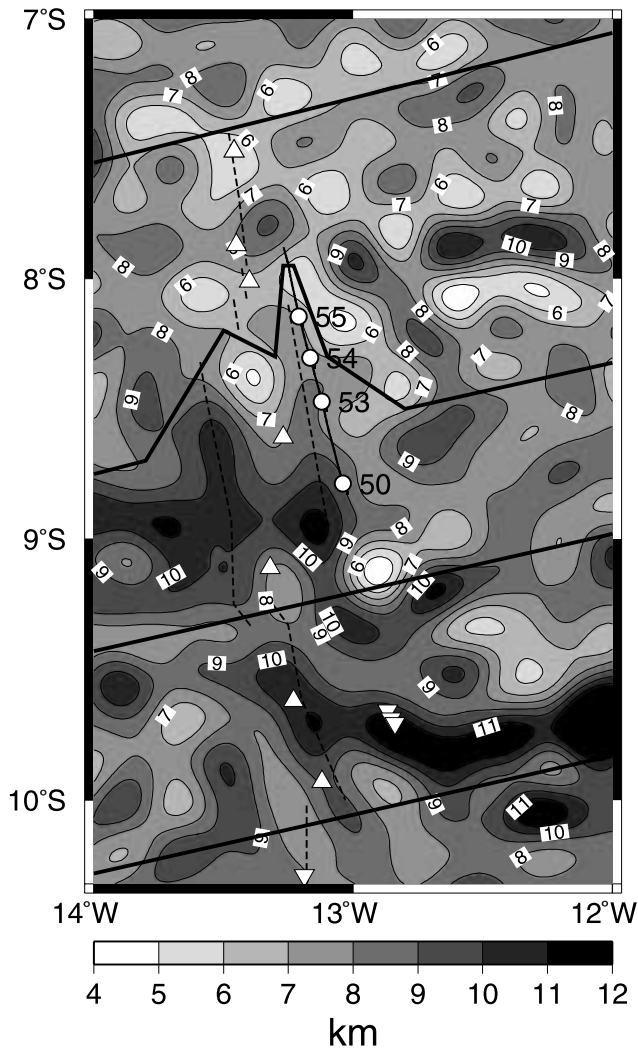


**Figure 12.** Crustal thickness variations required to explain the residual gravity anomalies of Figure 11, assuming no lateral variations in crustal or upper mantle density. Contour interval is 1 km. Thick solid and dashed lines are as in Figure 11a. Thinner solid line is the seismic line of *Minshull et al.* [1998], white circles are sonobuoy locations, triangles are the dredge sites of *Schilling et al.* [1985], and inverted triangles those of *Bourdon and Hémond* [2001].

the crust (Figure 12) [e.g., *Kuo and Forsyth*, 1988]. Unrealistic short-wavelength variations in crustal thickness were removed by low-pass filtering the data prior to downward continuation using a cosine taper between 25 and 45 km.

[29] The inferred crustal thickness varies along-axis from  $\sim 6$  km near the Ascension Fracture Zone to  $\sim 11$  km at the centers of segments A2 and A3, where the ridge axis is  $\sim 1.5$ – $2.0$  km shallower than in segment A1 (Figure 13). These crustal thickness variations are smaller than those required for Airy isostatic balance of the topography (Figure 13a), suggesting that the topography is partly maintained by the flexural strength of the axial lithosphere. Variations in axial depth are exaggerated because the bathymetry is sampled in a deep valley in segment A1, but on highs in segments A2 and A3. If a crustal density of  $2.8 \text{ mg/m}^3$  is assumed instead, thickness variations are reduced by only a

few hundred meters (Figure 13c). If the crustal density is assumed to vary with crustal thickness according to the relationship derived by *Minshull* [1996], the inferred thickness variations are almost identical because the density varies little for crustal thicknesses greater than 6 km.

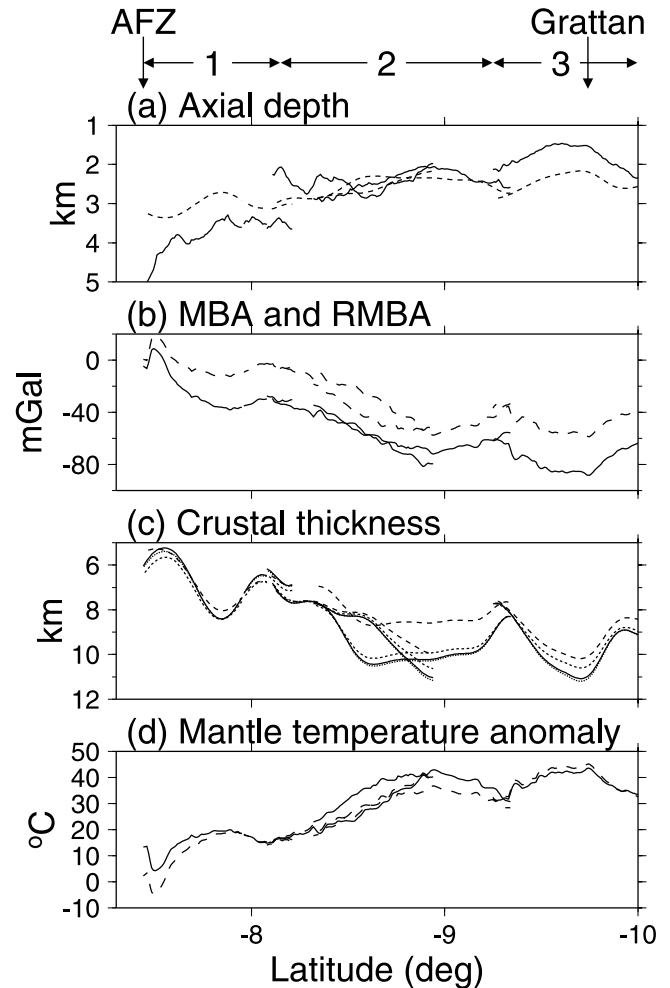


**Figure 13.** (a) Solid line marks axial depth sampled from the smoothed bathymetric data set of Figure 1a at the ridge axis as defined in Figure 1b. Both ridge axes are sampled in segment A2. Dashed line marks axial depth required to isostatically balance crustal thickness variations of Figure 12. AFZ is the Ascension Fracture Zone. (b) Solid line is the MBA of Figure 11a and dashed line is the RMBA of Figure 11b. Both are sampled as in (a). For ease of comparison, a constant shift is applied to the RMBA, since the absolute level is arbitrary. (c) Solid line is crustal thickness from Figure 12. Dotted line is crustal thickness for a model in which crustal density varies as a function of crustal thickness according to the fit of *Minshull* [1996]. Short dashed line is the inferred crustal thickness for a crustal density of  $2.80 \text{ Mg/m}^3$ . Longer dashed line is the crustal thickness inferred from the MBA using the approach of *Ito and Lin* [1995b] (see text). (d) Dashed line marks mantle temperature anomaly inferred from the MBA using the empirical relationship of *Ito and Lin* [1995a]. Solid line marks the result of applying the same relationship to the RMBA instead. In both cases, the absolute level is arbitrary.

However, this relationship often fails at segment boundaries, so inferred thicknesses close to such boundaries should not be considered reliable.

[30] An alternative approach to estimating the axial crustal thickness is to assume that contributions to the gravity anomaly from crustal thickness and mantle density variations are related through mantle temperature, since increased mantle temperatures cause increased decompression melting and therefore increased crustal thickness. Such an approach was applied to the Galapagos spreading center by *Ito and Lin* [1995b], who imposed a temperature anomaly at the base of the three-dimensional passive flow model of *Phipps Morgan and Forsyth* [1988], set at 160 km depth, estimated the crustal thickness produced using the linear melting function and depth–solidus relation of *Reid and Jackson* [1981], and showed that for such a model, 70–75% of the MBA comes from crustal thickness variations and 25–30% from mantle temperature variations. The along-axis slopes of the MBA and RMBA differ little except near significant ridge offsets, so the result of such an approach is that inferred along-axis crustal thickness variations are significantly less than those inferred from downward continuation of the RMBA (Figure 13c). Application of this approach to a variety of spreading rates gave the empirical relationship

$$\Delta T = -(0.0017U + 0.45)\Delta\text{MBA}$$

where  $U$  is the spreading rate in mm/yr,  $\Delta T$  is measured in °C and the MBA is measured in mGal [*Ito and Lin*, 1995a]. If the axial crustal thickening in segments A2 and A3 is attributed to the presence of hot mantle plume material beneath the axis, direct application of this relationship suggests a maximum mantle temperature anomaly of  $\sim+40^\circ\text{C}$  (Figure 13d). This value is slightly misleading since the MBA, and hence the inferred temperature, is depressed by the thermal edge effect of the Ascension Fracture Zone. Application of the same empirical relationship to the RMBA instead suggests that this effect contributes  $\sim+10^\circ\text{C}$  toward the inferred anomaly.

[31] The two approaches to estimating crustal thickness can in principle be distinguished where seismic constraints are available. A wide-angle seismic line was acquired close to the ridge axis in segment A2. The acquisition and modeling procedure are described by *Minshull et al.* [1998], who also show representative data. Moho depths are constrained by wide-angle reflections in three places on the line (Figure 14). Neither gravity-based model entirely fits the seismically derived crustal thicknesses within their likely uncertainties (Figure 14). However, the maximum variation in seismic crustal thickness of  $\sim 4$  km is much better matched by the model of Figure 12, which also gives  $\sim 4$  km of variation, than by the model based on *Ito and Lin's* [1995b] approach, which gives a variation of only  $\sim 3$  km.

## 6. Discussion

[32] The above analysis appears to preclude the presence of a region of anomalously hot material beneath the ridge axis extending beyond 160 km depth as a cause of the axial depth and gravity anomalies between the Ascension and the Bode Verde fracture zones. A more depth-limited thermal

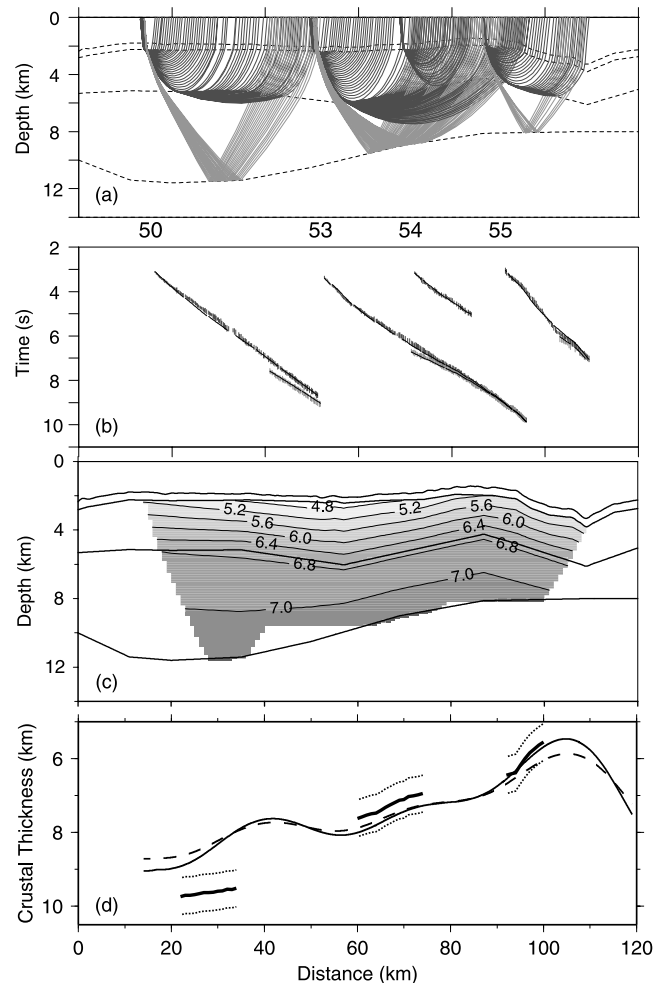


**Figure 14.** (a) Ray coverage for arrivals picked from the four sonobuoys marked in Figure 12. Numbered sonobuoy locations are marked beneath. Every 10th ray is plotted. Along-profile sonobuoy drift inferred from direct and seabed reflected arrivals is accounted for by binning receiver locations [*Bruguier and Minshull*, 1997]. (b) Vertical gray bars mark travel time picks with their uncertainties. Solid lines mark travel times predicted from the rays traced in (a). (c) Velocity contour plot for the region of the model constrained by seismic data. (d) Thin solid line marks crustal thickness variation sampled from Figure 12 along the seismic profile. Dashed line marks crustal thickness variation estimated from the MBA assuming 70% of the axial MBA variation comes from crustal thickness variations. Thick solid lines mark well-constrained crustal thickness from the seismic model of *Minshull et al.* [1998], with dotted lines marking estimated  $\pm 0.5$  km error bounds on these values.

anomaly cannot be excluded, but this anomaly would have to extend close to the base of the melting zone (perhaps at 60–80 km depth) to generate the observed crustal thickness anomalies. The axial depth, MBA, crustal thickness, and inferred temperature anomalies are all of comparable magnitude to those resulting at the Cocos Ridge from the off-axis Galapagos hot spot [*Ito and Lin*, 1995b], but are much shorter in wavelength. The  $\sim 450$  km along-axis width of

the bathymetric anomaly is also much less than that predicted by the simple inverse relation to spreading rate predicted by Ito and Lin [1995a], though a narrower ridge axis anomaly would be consistent with their model if the plume channel width were much reduced.

[33] Further constraints on the melting process in the Ascension region come from the chemistry of erupted basalts. Schilling *et al.* [1985] showed that basalts dredged from this region (Figure 12) are enriched in incompatible trace elements relative to normal MORB. La/Sm ratios reach values similar to those measured close to the Galapagos hot spot by Verma *et al.* [1983], though as with the geophysical anomalies, the wavelength of the anomaly is much shorter. Although this enrichment could occur during melt generation, very small melt fractions would be required, and it is therefore attributed to a similar enrichment in the mantle source region. Lead isotopic data [Hanan *et al.*, 1986; Bourdon and Hémond, 2001] also indicate significant enrichment of the mantle source in segments A1–A3, though He, Sr, and Nd isotopes fall mainly within the MORB field [Graham *et al.*, 1992; Fontignie and Schilling, 1996; Bourdon and Hémond, 2001]. Thus, the geochemical data suggest that the mantle source region is enriched in incompatible elements, but that this enrichment does not represent a primitive mantle source.

[34] Both geochemical and crustal thickness anomalies may be explained by the melting of a small mantle heterogeneity which has risen into the melting region at or close to the ridge axis in the Ascension area. Such a heterogeneity may be indistinguishable from the surrounding mantle in terms of rheology and density, but may be enriched in volatiles and therefore have a lower solidus temperature than the surrounding mantle, leading to initiation of melting at greater depth and to greater melt production than for a normal mantle peridotite [e.g., Bonatti, 1990]. A similar mechanism has been suggested for other areas of the Mid-Atlantic Ridge with elevated Pb isotopic and incompatible trace element ratios and anomalous bathymetry, at 33°S, 14°N and 35°N [Michael *et al.*, 1994; Bougault *et al.*, 1988; Dosso *et al.*, 1991; Niu *et al.*, 2001]. The scale of heterogeneity required is likely to be smaller than the ~200 km along-axis length of significantly elevated topography, because of dispersion during melt transport, along-axis channeling of asthenospheric flow, and along-axis transport of melt. Ultimately, there may be little observable difference between the effects a chain of such anomalies and those of a weak and intermittent off-axis plume which is channeled toward the ridge axis.

## 7. Conclusions

[35] From an analysis of bathymetric and potential field data for the Mid-Atlantic Ridge between 7° and 12°S, we conclude that:

1. The crustal accretion process has been strongly modified by anomalies in the mantle. The magmatically inflated segment A2 has been propagating northward at the expense of segment A1, and excess volcanism in segment A3 has created a large ridge-centered volcano, analogous to Axial Volcano on the Juan de Fuca Ridge.

2. Forward modeling of magnetic anomalies, combined with the interpretation of swath bathymetric data, suggests

that the spreading center at segment A2 is marked by a shallow rift valley, and not by the adjacent linear ridge where the inferred magnetization is largest.

3. The position and shape of large “bull’s-eye” gravity anomalies at segments A2 and A3 support the tectonic interpretation based on bathymetric and magnetic data. Data from segment A2 indicate that, if the ridge jump there occurred as recently as our magnetic modeling suggests, this jump is the surface expression of a longer-lived displacement of mantle upwelling at depth.

4. Along-axis gravity anomalies may be explained entirely by crustal thickness variations, with no evidence for significant mantle temperature variations. If a mantle plume is present in the region, its thermal effects are not significant at the ridge axis, despite significant effects on crustal thickness and composition.

5. In common with other parts of the Mid-Atlantic Ridge, geophysical and geochemical anomalies may be attributed to the arrival in the melting region of small mantle heterogeneities with lower solidus temperatures.

[36] **Acknowledgments.** Data acquisition was funded by the Office of Naval Research. We thank the officers, crew, and scientific parties of R/V *Robert Conrad* cruise 2601 and RRS *James Clark Ross* 05 for their assistance with data acquisition. NJB was supported by a NERC research studentship, TAM by a Royal Society University Research Fellowship, and JMB under Office of Naval Research 6.1 funding (program element 61153N). We thank Donna Blackman for a constructive review.

## References

- Bijwaard, H., and W. Spakman, Tomographic evidence for a narrow whole mantle plume below Iceland, *Earth Planet. Sci. Lett.*, **166**, 121–126, 1999.
- Bonatti, E., Not so hot “hot spots” in the oceanic mantle, *Science*, **250**, 107–110, 1990.
- Bougault, H., L. Dmitriev, J.-G. Schilling, A. Sobolev, J. L. Joron, and H. D. Needham, Mantle heterogeneity from trace elements: MAR triple junction near 14°N, *Earth Planet. Sci. Lett.*, **88**, 27–36, 1988.
- Bourdon, E., and C. Hémond, Looking for the “missing endmember” in South Atlantic Ocean mantle around Ascension Island, *Mineral. Petrol.*, **71**, 127–138, 2001.
- Brozena, J. M., Temporal and spatial variability of seafloor spreading processes in the northern South Atlantic, *J. Geophys. Res.*, **91**, 497–510, 1986.
- Brozena, J. M., and R. S. White, Ridge jumps and propagations in the South Atlantic Ocean, *Nature*, **348**, 149–152, 1990.
- Bruguier, N. J., and T. A. Minshull, Accurate modelling of sonobuoy refraction data to determine velocity variations in oceanic crust, *Mar. Geophys. Res.*, **19**, 25–36, 1997.
- Cande, S. C., and D. V. Kent, A new geomagnetic polarity time scale for the Late Cretaceous and Cenozoic, *J. Geophys. Res.*, **97**, 13,917–13,951, 1992.
- Cande, S. C., and D. V. Kent, Revised calibration of the geomagnetic polarity timescale for the Late Cretaceous and Cenozoic, *J. Geophys. Res.*, **100**, 6093–6095, 1995.
- Carlson, R. L., and C. N. Herrick, Densities and porosities in the oceanic crust and their variations with depth and age, *J. Geophys. Res.*, **95**, 9153–9170, 1990.
- Chen, Y., and W. J. Morgan, Rift valley/no rift valley transition at mid-ocean ridges, **1**, *J. Geophys. Res.*, **95**, 17,571–17,583, 1990.
- Davies, G. F., Ocean bathymetry and mantle convection, **1**, Large-scale flow and hotspot, *J. Geophys. Res.*, **93**, 10,467–10,480, 1988.
- Delaney, J. R., H. P. Johnson, and J. L. Karsten, The Juan de Fuca Ridge-hot spot-propagating rift system: New tectonic, geochemical and magnetic data, *J. Geophys. Res.*, **86**, 11,747–11,750, 1981.
- DeMets, C., R. G. Gordon, D. F. Argus, and S. Stein, Effect of recent revisions to the geomagnetic reversal timescale on estimates of current plate motions, *Geophys. Res. Lett.*, **21**, 2191–2194, 1994.
- Dosso, L., B. Hanan, H. Bougault, J.-G. Schilling, and J. L. Joron, Sr-Nd-Pb geochemical morphology between 10° and 17°N on the Mid-Atlantic Ridge: A new MORB isotope signature, *Earth Planet. Sci. Lett.*, **106**, 29–43, 1991.
- Fontignie, D., and J. G. Schilling, Mantle heterogeneities beneath the South Atlantic: A Nd-Sr-Pb isotope study along the Mid-Atlantic Ridge (3°S–46°S), *Earth Planet. Sci. Lett.*, **142**, 209–221, 1996.

- Graham, D. W., W. J. Jenkins, J. G. Schilling, G. Thomson, M. D. Kurtz, and S. E. Humphris, Helium isotope geochemistry of mid-ocean ridge basalts from the South Atlantic, *Earth Planet. Sci. Lett.*, *110*, 133–147, 1992.
- Grindlay, N. R., P. J. Fox, and K. C. Macdonald, Second-order ridge axis discontinuities in the South Atlantic: Morphology, structure and evolution, *Mar. Geophys. Res.*, *13*, 21–49, 1991.
- Hanan, B. B., R. H. Kingsley, and J. G. Schilling, Migrating ridge-hotspot interactions: Pb isotope evidence in the South Atlantic, *Nature*, *322*, 137–144, 1986.
- Heirtzler, J. R., G. O. Dickson, E. M. Herron, W. C. Pitman, and X. LePichon, Marine magnetic anomalies, geomagnetic field reversals, and motions of the ocean floor and continents, *J. Geophys. Res.*, *73*, 2119–2136, 1968.
- Hey, R., F. K. Duennebie, and W. J. Morgan, Propagating rifts on mid-ocean ridges, *J. Geophys. Res.*, *85*, 3647–3658, 1980.
- International Seismological Centre, *On-Line Bulletin*, Int. Seismol. Cent., Thatcham, UK, 2001. (Available at <http://www.isc.ac.uk/Bull>).
- Ito, G., and J. Lin, Oceanic spreading center-hotspot interactions: Constraints from along-isochron bathymetric and gravity anomalies, *Geology*, *23*, 657–660, 1995a.
- Ito, G., and J. Lin, Mantle temperature anomalies along the present and paleoaxes of the Galapagos Spreading Center as inferred from gravity analyses, *J. Geophys. Res.*, *100*, 3733–3745, 1995b.
- Johnson, H. P., and R. W. Embley, Axial Seamount: An active ridge axis volcano on the central Juan de Fuca Ridge, *J. Geophys. Res.*, *95*, 12,689–12,696, 1990.
- Kincaid, C., J.-G. Schilling, and C. Gable, The dynamics of off-axis plume-ridge interaction in the uppermost mantle, *Earth Planet. Sci. Lett.*, *137*, 29–43, 1996.
- Klingelhoefer, F., T. A. Minshull, D. K. Blackman, P. Harben, and V. Childers, Crustal structure of Ascension Island from wide-angle seismic data: Implications for the formation of volcanic islands, *Earth Planet. Sci. Lett.*, *190*, 41–56, 2001.
- Kuo, B. Y., and D. W. Forsyth, Gravity anomalies of the ridge-transform system in the South Atlantic between 31° and 34.5°S: Upwelling centres and variations in crustal thickness, *Mar. Geophys. Res.*, *10*, 205–232, 1988.
- LaBrecque, J. L., D. V. Kent, and S. C. Cande, Revised magnetic polarity time scale for Late Cretaceous and Cenozoic time, *Geology*, *5*, 330–335, 1977.
- Macdonald, K. C., P. J. Fox, L. J. Perram, M. F. Eisen, R. M. Haymon, S. P. Miller, S. M. Carbotte, M.-C. Cormier, and A. N. Shor, A new view of the mid-ocean ridge from the behaviour of ridge-axis discontinuities, *Nature*, *335*, 217–225, 1988.
- Malamud, B. D., and D. L. Turcotte, How many plumes are there?, *Earth Planet. Sci. Lett.*, *174*, 113–124, 1999.
- Mello, S. L. M., Marine geology and geophysics of the Mid-Atlantic Ridge between Ascension and St. Helena Islands, M.Sc. thesis, Univ. of Rio de Janeiro, Brazil, 1993.
- Michael, P. J., et al., Mantle control on a dynamically evolving spreading centre: Mid-Atlantic Ridge 31–34°S, *Earth Planet. Sci. Lett.*, *121*, 451–468, 1994.
- Miller, S. P., and R. N. Hey, Three-dimensional magnetic modelling of a propagating rift, Galapagos 95°30'W, *J. Geophys. Res.*, *91*, 3395–3406, 1986.
- Minshull, T. A., Along-axis variations in oceanic crustal density and their contribution to gravity anomalies at slow-spreading ridges, *Geophys. Res. Lett.*, *23*, 849–852, 1996.
- Minshull, T. A., N. J. Bruguier, and J. M. Brozena, Ridge-plume interactions or mantle heterogeneity near Ascension Island?, *Geology*, *26*, 115–118, 1998.
- Naar, D. F., and R. N. Hey, Fast rift propagation along the East Pacific Rise near Easter Island, *J. Geophys. Res.*, *91*, 3425–3438, 1986.
- Niu, Y., D. Bideau, R. Hékinian, and R. Batiza, Mantle compositional control on the extent of mantle melting, crust production, gravity anomaly, ridge morphology, and ridge segmentation: A case study at the Mid-Atlantic Ridge 33–35°N, *Earth Planet. Sci. Lett.*, *186*, 383–399, 2001.
- O'Connor, J. M., P. Stoffers, P. van den Bogaard, and M. McWilliams, First seamount age evidence for significantly slower African plate motion since 19 to 30 Ma, *Earth Planet. Sci. Lett.*, *171*, 575–589, 1999.
- Parker, R. L., The rapid calculation of potential anomalies, *Geophys. J. R. Astron. Soc.*, *31*, 447–455, 1973.
- Parker, R. L., and S. P. Huestis, The inversion of magnetic anomalies in the presence of topography, *J. Geophys. Res.*, *79*, 1587–1593, 1974.
- Parsons, B., and J. G. Sclater, An analysis of the variation of ocean floor bathymetry and heat flow with age, *J. Geophys. Res.*, *82*, 803–827, 1977.
- Phipps Morgan, J., and D. W. Forsyth, Three-dimensional flow and temperature perturbations due to a transform offset: Effects on oceanic crustal and upper mantle structure, *J. Geophys. Res.*, *93*, 2955–2966, 1988.
- Reid, I., and H. R. Jackson, Oceanic spreading rate and crustal thickness, *Mar. Geophys. Res.*, *5*, 165–172, 1981.
- Sandwell, D. T., and W. H. F. Smith, Marine gravity anomaly from Geosat and ERS-1 satellite altimetry, *J. Geophys. Res.*, *102*, 10,039–10,054, 1997.
- Schilling, J. G., Fluxes and excess temperatures of mantle plumes inferred from their interaction with mid-ocean ridges, *Nature*, *352*, 397–403, 1991.
- Schilling, J. G., G. Thomson, R. Kingsley, and S. Humphris, Hotspot-migrating ridge interaction in the South Atlantic, *Nature*, *313*, 187–191, 1985.
- Shen, Y., S. C. Solomon, I. Th. Bjarnason, and C. J. Wolfe, Seismic evidence for a lower mantle origin of the Iceland plume, *Nature*, *395*, 62–65, 1998.
- Shirey, S. B., J. F. Bender, and C. H. Langmuir, Three-component isotopic heterogeneity near the Oceanographer transform, Mid-Atlantic Ridge, *Nature*, *325*, 217–223, 1987.
- Sleep, N. H., Tapping of magmas from ubiquitous mantle heterogeneities: An alternative to mantle plumes?, *J. Geophys. Res.*, *89*, 10,029–10,041, 1984.
- Small, C., Observations of ridge-hotspot interactions in the Southern Ocean, *J. Geophys. Res.*, *100*, 17,931–17,946, 1995.
- Tucholke, B. E., J. Lin, M. C. Kleinrock, M. A. Tivey, T. B. Reed, J. Goff, and G. E. Joroslów, Segmentation and crustal structure of the western Mid-Atlantic Ridge flank, 25°25'–27°10'N and 0–29 m.y., *J. Geophys. Res.*, *102*, 10,203–10,223, 1997.
- van Andel, Tj. H., and G. R. Heath, Tectonics of the Mid-Atlantic Ridge, 6–8° south latitude, *Mar. Geophys. Res.*, *1*, 5–36, 1970.
- Verma, S. P., J.-G. Schilling, and D. G. Waggoner, Neodymium isotopic evidence for Galapagos hotspot-spreading centre evolution, *Nature*, *306*, 654–657, 1983.
- Vogt, P. R., Amplitude of oceanic magnetic anomalies and chemistry of oceanic crust: Synthesis and review of “magnetic telechemistry”, *Can. J. Earth Sci.*, *16*, 2236–2262, 1979.
- Wolfe, C. J., I. Th. Bjarnason, J. C. VanDecar, and S. C. Solomon, Seismic structure of the Iceland mantle plume, *Nature*, *385*, 245–247, 1997.

N. J. Bruguier, Pembroke College, Trumpington Street, Cambridge CB2 1RF, UK. (ca4@pem.cam.ac.uk)

T. A. Minshull, Southampton Oceanography Centre, Southampton SO14 3ZH, UK. (tmin@soc.soton.ac.uk)

J. M. Brozena, Marine Geosciences Division, Code 7421, Naval Research Laboratory, 4555 Overlook Avenue SW, Washington, DC 20375, USA. (john@qr.nrl.navy.mil)